Journal of Power Sources 453 (2020) 227844

Contents lists available at ScienceDirect

Journal of Power Sources

journal homepage: www.elsevier.com/locate/jpowsour

High-power, non-enzymatic glucose biofuel cell based on a nano/micro hybrid-structured Au anode

Tien-Fu Chu [a], Raja Rajendran [b], Iren Kuznetsova [c], Gou-Jen Wang [a,d,*]

[a] Department of Mechanical Engineering, National Chung-Hsing University, Taichung, Taiwan
[b] Department of Physics, National Chung-Hsing University, Taichung, Taiwan
[c] Kotelnikov Institute of Radio Engineering and Electronics, Russian Academy of Science, Russia
[d] Graduate Institute of Biomedical Engineering, National Chung-Hsing University, Taichung, Taiwan

HIGHLIGHTS

- We develope a high-power non-enzymatic glucose biofuel cell.
- The novel anode consists of a micro/nano hybrid structure of gold.
- The monolayer of Au nanoparticles significantly enhances the glucose oxidation.
- The current density of 29.5 mA/cm^2 occurs at the power density of 10.7 mW/cm^2.
- The energy conversion efficiency was calculated to be 52.47%.

ARTICLE INFO

Keywords:
Non-enzymatic glucose biofuel cell
Nano/micro hybrid-structured anode
Self-assembled monolayer of Au nanoparticles

ABSTRACT

In this study, a high-power, non-enzymatic glucose biofuel cell (GBFC) based on a nano/micro hybrid-structured Au anode is proposed. A uniformly distributed micro-hemispheric array of polycarbonate is fabricated for this novel electrode by hot embossing using a Ni mold. The nano/micro hybrid-structured Au anode is then fabricated by depositing an Au nanoparticle monolayer on the micro-hemispheric array using 1,6-hexanedithiol as a two-sided anchor. The cathode is composed of a graphene film-coated glassy carbon electrode. Nafion, a proton exchange membrane, is used to separate the anode and cathode and complete the battery assembly. Experimental results demonstrate that the proposed non-enzymatic GBFC has a high-power density of 10.7 mWcm^{-2}, a high current density of 29.5 mAcm^{-2}, an open-circuit voltage of 8.2 V, and a shorted-circuit current of 34 mA at room temperature. The energy conversion efficiency of the electrode is calculated to be 52.47%. In addition, the proposed GBFC possesses advantages such as ease of production on a large scale, low manufacturing cost, high repeatability, and long-term preservation. Therefore, it is highly feasible for commercialization and use in practical applications.

1. Introduction

Biofuel cells (BFCs) [1], a form of "green" energy generators, have attracted considerable attention. These cells can generate electricity directly from the oxidation of biological organic matter. BFCs can generally be divided into two categories according to the type of catalyst used: microbial biofuel cells (MFCs) [2] and enzymatic biofuel cells (EFCs). MFCs generate electricity using bacteria and mimic bacterial interactions found in nature. This type of BFC has been employed in many useful applications, such as wireless sensor networks [3], energy recovery [4,5], and toxic metal elimination during wastewater treatment [6]. EFCs use enzymes as a catalyst to oxidize their fuel [7,8].

Glucose is recognized as the most essential energy source for many living organisms. During energy metabolism, glucose is generally oxidized to CO_2 and water, and this process simultaneously generates adenosine triphosphate to provide energy to drive various processes in living cells. During these oxidation processes, glucose can generate up to 16 kW/g energy and 12 electrons/molecule [9]. Due to its advantages, such as natural abundance, renewability, non-toxicity, and ease of production, glucose is a useful fuel for BFCs. The first glucose biofuel cell

* Corresponding author. Department of Mechanical Engineering, National Chung-Hsing University, Taichung, Taiwan.
E-mail address: gjwang@dragon.nchu.edu.tw (G.-J. Wang).

https://doi.org/10.1016/j.jpowsour.2020.227844
Received 25 October 2019; Received in revised form 2 January 2020; Accepted 4 February 2020
Available online 5 March 2020
0378-7753/© 2020 Elsevier B.V. All rights reserved.

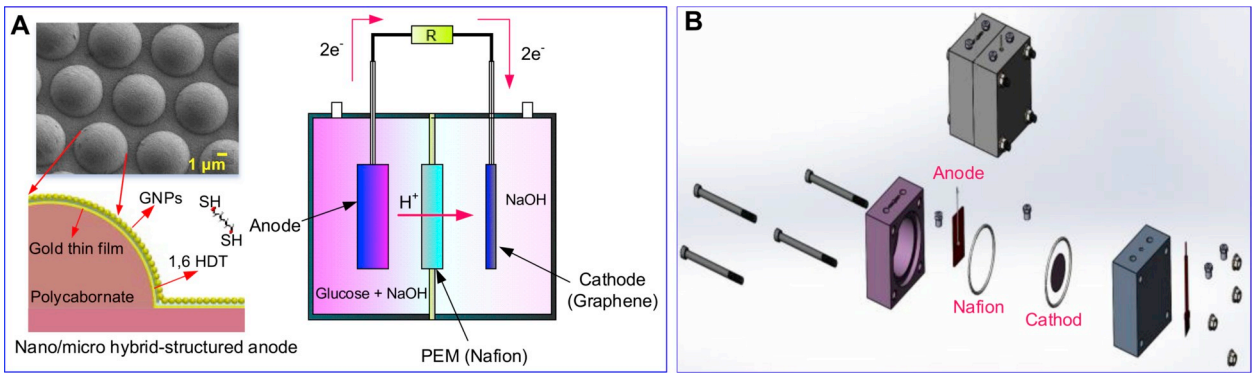

Fig. 1. (A) Schematic of the proposed non-enzymatic glucose biofuel cell based on a nano/micro hybrid-structured Au anode. (B) Components of the biofuel cell.

(GBFC) was presented in 1964 and had a glucose oxidase bio anode and a Pt cathode to indirectly convert the chemical energy of glucose into electricity [10]. Since then, GBFCs have attracted wide attention due to the rapid development of wearable or implantable medical devices [11–14].

GBFCs can be divided into enzymatic- and non-enzymatic-type cells. Enzymatic GBFCs utilize enzymes, such as glucose oxide, to catalyze the oxidation of glucose, and/or reduction of oxygen or peroxide and convert chemical energy into electricity. Due to the excellent selectivity and reaction rate of specific enzymes, enzyme-based GBFCs are the main focus of current development efforts [15–21]. However, enzyme-based GBFCs suffer from a number of disadvantages, such as the potential for poisoning, limited enzyme stability, and cumbersome enzyme immobilization procedures [12]. Degradation of enzyme activity poses another problem for long-term applications. Therefore, non-enzymatic technologies that use nanostructures incorporating noble metals and their related composites as catalysts without the need for additional enzymes have gradually emerged as a new development trend [22–24].

Due to their ability to catalyze glucose oxidation, Pt and its alloys have been widely used as catalysts in non-enzymatic GBFCs [25–27]. High-power density, high open-circuit voltage (V_{oc}), and long-term usability are among the benefits of this type of catalyst. However, in addition to their relatively high cost, Pt based anodes are easily affected by interferences and could generate an oxide layer that may degrade their power output and reduce their efficiency. Therefore, the oxides of other metals, such as Au, Ag, and Ni, which present better long-term stability compared with Pt, have been employed as anodes in GBFCs [28–31]. Carbon-based materials, including carbon, carbon nanotubes, and graphene, are alternative catalysts for GBFCs [32–35]. Among non-Pt based metals, Au, which features high electro catalytic capability for glucose oxidation and oxygen reduction, is a suitable substitute for Pt in alkaline glucose fuel cells [28]. Compared with other metals, Au has a more negative oxidation potential in neutral and alkaline media. Xu et al. [30] proposed nanoporous Au (NPG) structures with abundant high-index facets, kinks, and steps as effective catalysts for glucose oxidation in GBFCs; these catalysts achieved a high current density of approximately 9 A cm^{-2} mg^{-1}, which is over 20-fold greater than the current density obtained from the Au nanoparticles devised by Turkevich under the same conditions. Yang et al. [31] proposed an anode composed of ultrathin Au nanowires for high-performance non-enzymatic glucose sensing and incorporated the same into a glucose/O_2 biofuel cell; here, a maximum power density of 126 μW cm^{-2}, V_{oc} of 0.425 V, and shorted-circuit current (I_{sc}) density of 1.34 mA cm^{-2} were obtained. Experimental results further showed that a maximum power density of 26.6 mW/cm^2 could be obtained at a current density of 89 mA cm^{-2} and temperature of 70 °C. Unfortunately, although this GBFC was favorable for large scale use, its fairly high operating temperature limited its applications. A self-sustained and compact drug delivery model with self-diagnosis and self-evaluation mechanisms featuring a glucose/O_2 fuel cell based biosensor was also proposed by Wang et al. [36]. The proposed device could provide a feasible *in vitro* "diagnosis–therapy–evaluation" platform for clinical cancer therapy.

Energy conversion in a GBFC highly depends on the effective catalytic area of the electrode. For actual applications, characteristics such as high energy conversion efficiency, low cost, long-term stability, ease of production, and high reproducibility are required. In this study, a high-power, non-enzymatic GBFC with high energy conversion efficiency, long-term stability, and low cost is proposed. A nano/micro hybrid-structured anode with uniformly distributed catalysts composed of a monolayer of Au nanoparticles based on a polycarbonate (PC) substrate was fabricated by hot embossing and self-assembly monolayer deposition. The nano/micro hybrid-structure largely enhanced the reaction area of the catalyst, and the monolayer Au particles facilitated the effective oxidation of glucose. Moreover, the PC substrate and hot embossing fabrication process reduced production costs.

2. Materials and methods

2.1. Structure of the proposed GBFC

Fig. 1 schematically illustrates the structure of the proposed non-enzymatic, alkaline GBFC based on a nano/micro hybrid-structured Au anode. The cell contained a nano/micro hybrid-structured Au anode, a graphene film-coated GC cathode, and a proton exchange membrane (Nafion) to separate the anode and cathode. A resistor was coupled to connect the anode and cathode and form a GBFC system. The nano/micro hybrid-structured Au anode featured a uniform monolayer of Au nanoparticles on an array of micro-hemispheres and significantly enhanced the catalytic efficiency of the cell for glucose; indeed, this anode is the key factor in this novel GBFC.

The chemical reactions of the proposed GBFC are as follows:

$$\textbf{Anode}: \ (A)C_6H_{12}O_6 + 2OH^- \rightarrow C_6H_{11}O_7^- + H_2O + H^+ + 2e^-$$
$$(B)C_6H_{12}O_6 + OH^- \rightarrow C_6H_{10}O_6 + H_2O + H^+ + 2e^-$$

$$\textbf{Cathode}: \ 1/2O_2 + 2H^+ + 2e^- \rightarrow H_2O$$

$$\textbf{Total}: \ (A)C_6H_{12}O_6 + 2OH^- + 1/2O_2 + 2H^+ \rightarrow C_6H_{12}O_7 + 2H_2O$$
$$(B)C_6H_{12}O_6 + OH^- + 1/2O_2 + H^+ \rightarrow C_6H_{10}O_6 + 2H_2O$$

2.2. Preparation of the nano/micro hybrid-structured Au anode

The fabrication process of the nano/micro hybrid-structured Au anode for the proposed GBFC is shown in Fig. S1; the complete process included photolithography, thermal melting, electroforming of the Ni mode, hot embossing, and Au nanoparticle deposition.

(1) Photolithography

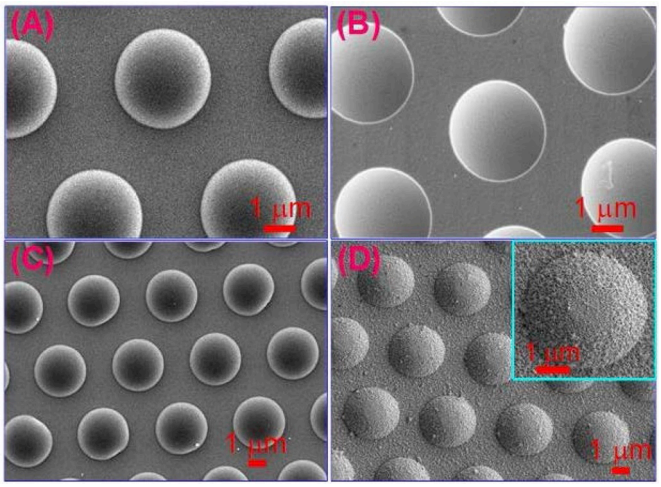

Fig. 2. SEM images of (A) the micro-hemispheric PR array obtained after photolithography, (B) the concave micro-hemispheric array on the Ni mold obtained by using electroforming, (C) the PC substrate obtained after hot embossing, and (D) the micro/nano hybrid-structured Au anode.

A 2 μm-thick positive photoresist (PR) (AZ 1518, Microchemicals, Germany) was spin-coated onto the surface of a 6-inch reclaimed silicon wafer. The PR-coated silicon wafer was then exposed by using a mask aligner (EVG, Austria) to transfer the pattern from the mask to the PR layer. The exposed PR was developed to obtain an array of PR cylinders. The diameter of each cylinder and the distance between any two cylindrical centers were 2 and 3 μm, respectively.

(2) Thermal melting

The silicon wafer with cylindrical PR array was placed on a 160 °C hot plate for thermal melting for 5 min, and the cylindrical PR array gradually became hemispherical in shape.

(3) Electroforming of the Ni mold

A Ni mold of the concave hemispherical array was fabricated by Hui-Fong Micro-Fabrication Technologies (Kaohsiung, Taiwan) through electroforming.

(4) Hot embossing

Hot embossing transferred the micro-hemispheric array onto a PC film using the fabricated Ni mold.

(5) Au nanoparticle deposition

An Au thin film was sputter-deposited onto the surface of the micro-structured PC substrate using a sputter coater (Model 108 Auto, Cressington, UK). The device was then dipped into 10 mM 1,6-hexanedithiol (1,6-HDT) solution for 18 h to enable one thio-end of the 1,6-HDT molecules to attach to the thin Au layer [37]. Afterward, a 10 wt% colloidal Au nanoparticle (GNP) solution was dropped onto the dithiol-modified electrode to obtain the micro/nano hybrid-structured Au anode.

2.3. Apparatus and measurement

Electrochemical experiments were carried out at room temperature (23 °C) using an EC-Lab SP-150 potentiostat (Bio-Logic Science Instruments, USA). The counter electrode, reference electrode, and working electrode were a graphene/GC cathode, saturated Ag/AgCl, and the fabricated nano/micro hybrid-structured Au anode, respectively.

3. Results and discussion

3.1. Morphology of the nano/micro hybrid-structured Au anode

Fig. 2 shows SEM images of the micro-hemispheric PR array after photolithography, the concave micro-hemispheric array on the Ni mold

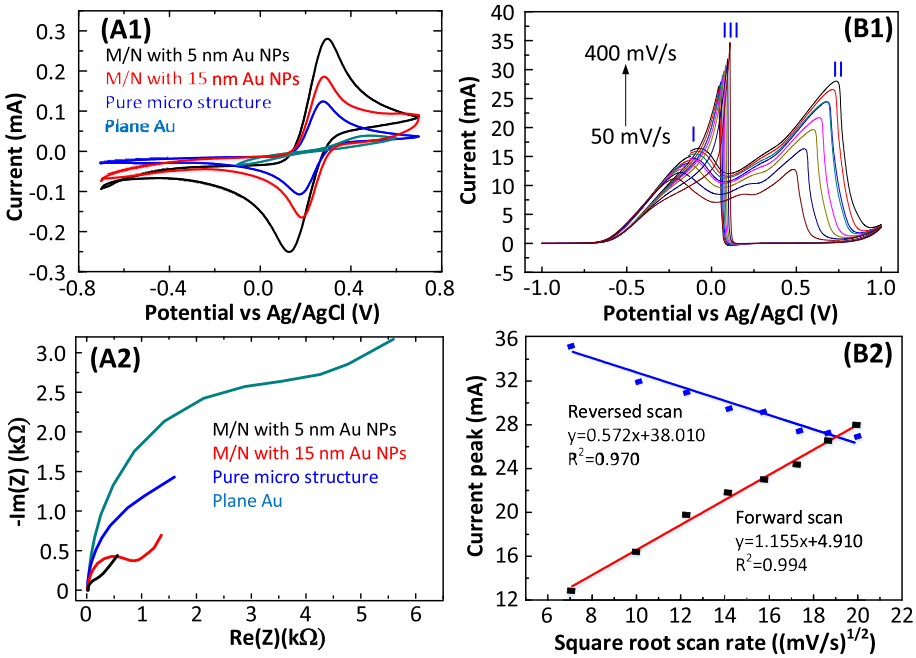

Fig. 3. (A) Electric characteristics of various electrodes: (1) Cyclic voltammograms and (2) Nyquist plots. (B) Characterization of the proposed electrode by cyclic voltammetry: (1) Cyclic voltammetry at various scan rates in 0.2 M NaOH solution containing 0.1 M glucose as the electrolyte. (2) Linear relationship between the redox peak currents and square root of the scan rate.

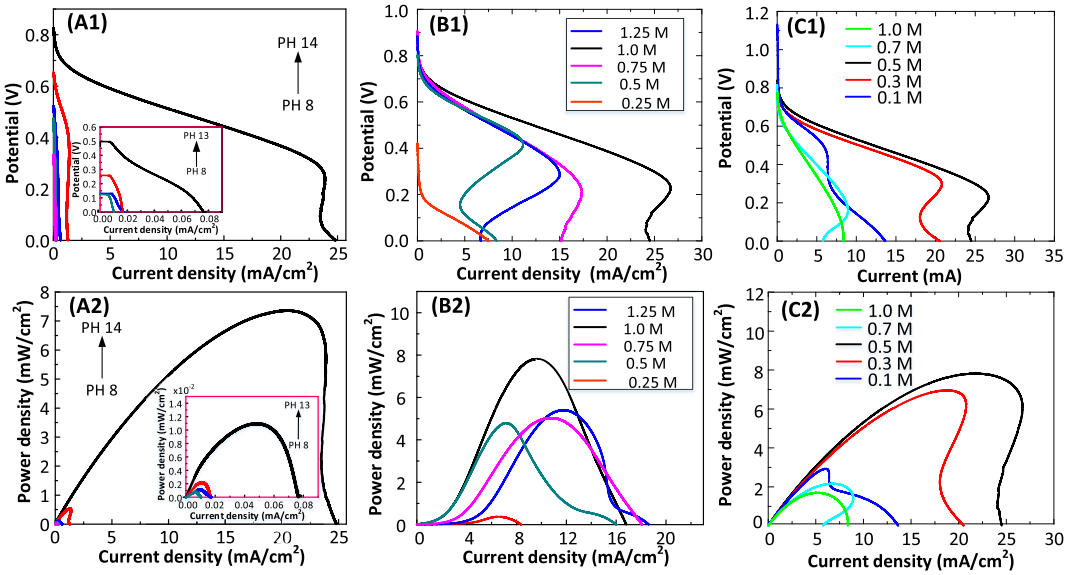

Fig. 4. (A) Effect of pH on the performance of the proposed GBFC: (1) Polarization and (2) power density curves. (B) Effect of NaOH concentration on the performance of the proposed GBFC: (1) Polarization and (2) power density curves. (C) Effect of glucose concentration on the performance of the proposed GBFC: (1) Polarization and (2) power density curves.

obtained by using electroforming, the PC substrate obtained after hot embossing, and the micro/nano hybrid-structured Au anode. Fig. 2(A) and (B) show that the micro-hemispheric PR array is well-arranged and successfully transferred to the Ni mold. Fig. 2(C) shows that the micro-hemispheric PR array was completely transferred to the PC substrate. Fig. 2(D) reveals that the Au nanoparticles are uniformly deposited on the PC substrate.

3.2. Electrochemical characteristics of the anode

(1) Electric characteristics

Two sizes of Au nanoparticles (i.e., 5 and 15 nm) were used to fabricate the micro/nano hybrid-structured Au anode. The electric characteristics of the two resulting anodes were investigated and compared with those of a pure micro-hemispheric array anode and a planar Au anode. Fig. 3(A) illustrates the cyclic voltammograms (Fig. 3 (A1)) and Nyquist plots (Fig. 3(A2)) of all four anodes. Cyclic voltammetry was conducted in phosphate buffer solution (PBS) with a potential sweep range of −0.7 V to 0.7 V under a scan rate of 50 mV/s. Nyquist plots were obtained by electrochemical impedance spectroscopy in PBS solution with an AC frequency range of 50 mHz to 50 kHz. The cyclic voltammogram in Fig. 3(A1) reveals that, among the anodes investigated, the micro/nano hybrid-structured Au anode with 5 nm Au nanoparticles possesses the highest redox capability, likely due to the increase in activation surface area provided by the uniform distribution of 5 nm Au nanoparticles on the electrode surface. Moreover, this anode showed the lowest charge transfer resistance (Fig. 3(A2)) and, hence, the best conductivity. The low resistance of this anode could also be attributed to the uniform distribution of 5 nm Au nanoparticles on the electrode surface. Therefore, the micro/nano hybrid-structured Au anode with 5 nm Au nanoparticles deposited on its surface was used as the anode for further fuel cell experiments.

(2) Effective surface area of the fabricated anode

Surface structure and roughness affect the reactions between the electrode surface and electrolyte and, hence, determine the glucose oxidation capability of the anode. Fig. S2 shows the steady-state cyclic voltammograms and corresponding I–t curves of the micro/nano hybrid-structured Au anode and planar Au electrode in 0.5 M H_2SO_4 at 20 mV/s versus those of a Ag/AgCl reference electrode; here, the I–t curves were transformed from the corresponding cyclic voltammograms. Since the charge required by an Au electrode to form 1 cm^2 of AuO is 386 μC, the effective surface area of an electrode can be estimated from the total amount of electric charge absorbed by the electrode in the reduction loop. The total amount of electric charge absorbed by the electrode was measured by integrating the area of the reduction loop in Fig. S2(B). The effective surface area of the micro/nano hybrid-structured Au anode and plane Au electrode were calculated to be 6.23 and 2.90 cm^2, respectively. Thus, the effective surface area of the micro/nano hybrid-structured Au anode was 2.17-fold greater than that of the plane Au electrode.

(3) Diffusion-controlled electrochemical reaction

If an electron is rapidly transferred between the electrode and electrolyte, then the reaction is dominated by diffusion control. A typical diffusion-controlled reaction can be confirmed by the Randles–Sevcik equation, which is commonly used to confirm the typical diffusion-controlled reaction. The Randles–Sevcik equation can be written as follows:

$$i_p = 2.69 \times 10^5 \times n^{3/2} \times A \times C \times D^{1/2} \times v^{1/2} \quad (1)$$

where i_p denotes the value of the peak current (A), n is the number of electrons appearing in a half-reaction of the redox couple, A is the area of the electrode (cm^2), C denotes the concentration of the analyte (mol/cm^3), D is the diffusivity of the analyte (cm^2/s), and v is the potential scan rate (V/s). In general, n, A, C, and D are fixed during a typical electrochemical reaction; therefore, i_p is proportional to the square root of the scan rate. Fig. 3(B)(1) shows the cyclic voltammograms of the proposed electrode at various scan rates ranging from 50 mV/s to 400 mV/s in 0.2 M NaOH solution containing 0.1 M glucose as the electrolyte. Three current peaks were observed; here: (I) D-glucose molecules were electrochemically adsorbed on the surface of the Au electrode through dehydrogenation; (II) the dehydrogenated molecules were then converted into D-gluconate ions by direct oxidation, and (III) the dehydrogenated glucose was oxidized to δ-gluconolactone [38]. Each of these three processes generates electrons. Furthermore, due to the enhanced effective surface area of the micro/nano hybrid-structured Au

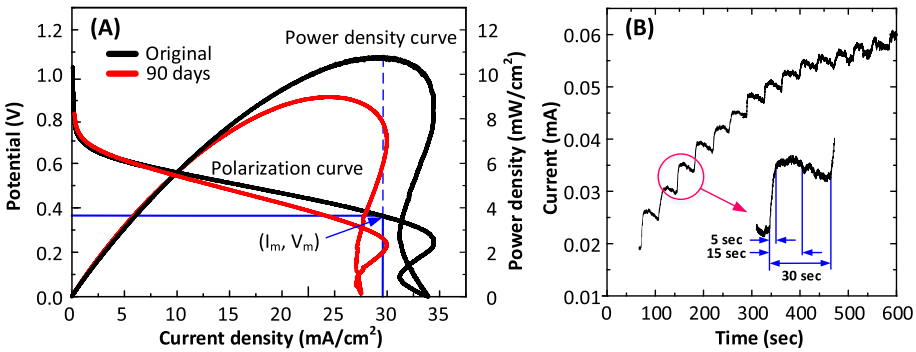

Fig. 5. (A) Polarization and power density curves of the proposed GBFC. (B) Amperometry results of successive additions of 0.1 M glucose for 30 s (applied potential, 0.45 V).

anode and the monolayer of Au nanoparticles on the electrode surface, the peak currents at (II) and (III) are relatively large.

The peak currents and peak potentials increased with increasing scan rate. The linear relationships between the forward peak and reversed peak current and the scan rate of the proposed electrode are shown in Fig. 3(B2). The peak current was linearly correlated with the square root of the scan rate. Thus, the proposed anode is typically diffusion-controlled.

3.3. Performance of the GBFC

3.3.1. Parameter optimization

To develop a highly efficient GBFC, we investigated the effects of electrolyte pH, NaOH concentration, and glucose concentration on the GBFC responses.

(1) Effect of pH

To investigate the effect of electrolyte pH on the redox behavior of the biofuel cell, we set the glucose concentration to 0.5 M and adjusted the pH of the electrolyte. Fig. 4(A) shows the polarization and power density curves of the GBFC at different pH values. The polarization and power density curves reveal that the proposed GBFC has maximum energy conversion at pH 14. The current density was maintained at a relatively low value of 2.6 mA/cm^2 from pH 8 to pH 13 and then sharply increased to 28 mA/cm^2 at pH 14. These results indicate that the proposed GBFC is an alkaline (pH 14) GBFC and that the mass transfer resistance could be successfully reduced.

(2) Effect of NaOH concentration

As demonstrated above, our GBFC is an alkaline GBFC. Besides pH, the concentration of the electrolyte (NaOH) could also affect the performance of the GBFC. The polarization and power density curves of the proposed GBFC at various NaOH concentrations and constant glucose concentration of 0.5 M are shown in Fig. 4. The polarization curves shown in Fig. 4(B1) illustrate that maximum efficiency with a V_{oc} of 0.89 V and I_{sc} of 24.8 mA could be achieved at 1.0 M NaOH. The power density curves shown in Fig. 4(B2) also indicate that an optimal power density of 7.9 mW/cm^2 could be obtained at 1.0 M NaOH.

At the cathode, NaOH produces OH^-, which has a mixing effect on the fuel cell because it increases the resistance of the fuel cell anode while reducing the cathodic effect of mass transfer. Therefore, the bioelectrical activity of the GBFC at the cathode peaks when the production of OH^- reaches saturation. In this study, the cathode was a graphene/GC electrode, which has a maximum power density of 7.9 mW/cm^2 at a NaOH saturation concentration of 1.0 M. The experimental results imply that the mass transfer of NaOH to OH^- is another factor influencing GBFC efficiency.

(3) Effect of glucose concentration

Investigation of the effect of glucose concentration on the GBFC responses was conducted under the conditions of pH 14 and 1.0 M NaOH. Fig. 4(C) shows the polarization and power density curves of the proposed GBFC at various glucose concentrations. The polarization curves in Fig. 4(C1) indicate that maximum efficiency with a V_{oc} of 0.89 V and I_{sc} of 24.8 mA could be obtained at 0.5 M glucose. Similarly, as shown in Fig. 4(C2), a maximum power density of 8.2 mW/cm^2 could be observed at 0.5 M glucose. In general, the power density of a GBFC increases with increasing glucose concentration; therefore, the power density gradually increases as the glucose concentration is increased from 0.1 M to 0.5 M. However, excess glucose molecules can completely cover the electrode surface such that no further oxidation can occur on it. In addition, an oversupply of glucose molecules hinders the transfer of H^+ from the electrode surface, thus reducing the power density of the electrode. In this study, 0.5 M glucose provided adequate molecules to completely cover the surface of the proposed micro/nano hybrid-structured anode.

3.3.2. GBFC performance

Using the optimized parameters of pH 14, 1.0 M NaOH, and 0.5 M glucose, the polarization, and power density curves of the proposed GBFC operated at room temperature are shown in Fig. 5(A). The polarization curve revealed that the V_{oc} and I_{sc} of our GBFC are 0.84 V and 34.45 mA, respectively. Compared with published results, these values are relatively high. The power density curve also demonstrates that a maximum current density of 30 mA/cm^2 occurs at a power density of 10.7 mW/cm^2. The current density of our proposed anode is also greater than those reported in most published studies. The energy conversion efficiency of an electrode can be calculated by using the following formula [39].

$$\eta = \frac{V_m \times I_m}{\text{Input power area}} 100\% \quad (2)$$

As shown in Fig. 5(A), I_m denotes the current density with respect to the peak of the power density curve, V_m is the potential corresponding to I_m at the polarization curve, and the input power area is the area below the polarization curve. The energy conversion efficiency of our anode was calculated to be 52.47%. Due to the high peak currents at points (II) and (III) in Fig. 3(B1), our anode achieved a relatively large I_m, which could lead to high conversion efficiency.

To further investigate the response time of glucose on the proposed anode, we conducted chronoamperometry. The micro/nano hybrid-structured anode was immersed in 0.1 M NaOH solution with continuous stirring, and a constant potential of 0.45 V was applied. The solution was stirred at 400 rpm at room temperature. Fig. 5(B) shows the amperometry results of the periodic addition of 0.1 M glucose to the proposed anode for 30 s. The amperometric currents responded rapidly with each addition of glucose.

Table 1
Performance comparison of recently developed nanostructure-based GBFCs.

Anode	V_{oc} (V)	Power output (mW/cm^2)	Current density (mA/cm^2)	Reference
FePt (NPs)	64	0.095	3.7	[19]
Pd–Pt/GA/NFP	Not provided	3.6	Not provided	[27]
Au nanowire	0.425	0.126	1.34	[31]
3D Pt/MWCNT	0.7	2.3	Not provided	[33]
NiO/GNS	0.756	Not provided	0.066	[34]
3D graphene NiO	1.1	13.48	Not provided	[35]
3D Pt_3Ni_7/MWCNT	0.786	3.12	14.94	[40]
NPG-PtBi	0.9	8	Not provided	[41]
3D Co_3O_4/MWNTs	0.68	0.22	1.46	[42]
Au Nanostructures	0.54	0.0146	2.7	[43]
Nano/micro hybrid Au	0.82	10.7	29.5	**This work**

As shown in Fig. 5(A), the power generation performance of the proposed GBFC was degraded by only <15% after storage in ambient air at room temperature for over 90 days.

Many GBFCs with nanostructure-based anodes have recently been investigated due to their numerous advantages, which include a large surface area, high catalytic efficiency, and high surface activity. The functional properties (i.e., V_{oc}, power output, and current density) of the proposed non-enzymatic GBFC were compared with those of other recently developed GBFCs, and the results are shown in Table 1. In general, the GBFC proposed in this study demonstrated better performance than other BFCs in terms of these functional properties.

4. Conclusions

GBFCs have attracted wide attention due to the rapid development of wearable or implantable medical devices. In this study, we developed a high-power, non-enzymatic GBFC based on a nano/micro hybrid-structured Au anode. The distinguishing feature of our anode is a monolayer of Au nanoparticles ($\varphi = 5$ nm) uniformly deposited on the electrode surface; hence, the glucose oxidation ability of our anode is significantly enhanced. Experimental results demonstrate that the V_{oc} and I_{sc} of our GBFC are 0.84 V and 34.45 mA, respectively. Compared with published results, these values are relatively high. A current density of 29.5 mA/cm^2, which is also greater than that reported in most of the available literature, occurred at a power density of 10.7 mW/cm^2. The energy conversion efficiency of our anode was calculated to be 52.47%. The proposed GBFC can easily be produced on a large scale, is of relatively low cost, has high repeatability, and can be preserved for long periods of time without great losses in performance. Therefore, our GBFC is highly feasible for commercialization and use in practical applications.

Declaration of competing interest

The authors report no conflicts of interest in this work.

Acknowledgement

The authors would like to offer their thanks to the Ministry of Science and Technology of Taiwan (grant # MOST-107-2923-E-005-001-MY3) and the Russian Foundation for Basic Research (grant # 18-29-23042) for their financial support of this research.

Appendix A. Supplementary data

Supplementary data to this article can be found online at https://doi.org/10.1016/j.jpowsour.2020.227844.

References

[1] M. Gamella, A. Koushanpour, E. Katz, Biofuel cells – activation of micro- and macro-electronic devices, Bioelectrochemistry 119 (2018) 33–42.
[2] A. Ebrahimi, G.D. Najafpour, D. Yousefi Kebria, Performance of microbial desalination cell for salt removal and energy generation using different catholyte solutions, Desalination 432 (2018) 1–9.
[3] V. Wang, S.L.Z. Cai, K. Sivakumar, Q. Zhang, S. Kjelleberg, B. Cao, S.C.J. Loo, L. Yang, A stable synergistic microbial consortium for simultaneous azo dye removal and bioelectricity generation, Bioresour. Technol. 155 (2014) 71–76.
[4] B. Filanovsky, E. Granot, I. Presman, I. Kuras, F. Patolsky, Long-term room-temperature hydrazine/air fuel cells based on low-cost nanotextured CueNi catalysts, J. Power Sources 246 (2014) 423–429.
[5] B. Zhang, C. Feng, J. Ni, J. Zhang, W. Huang, W. Huang, Simultaneous reduction of vanadium (V) and chromium (VI) with enhanced energy recovery based on microbial fuel cell technology, J. Power Sources 204 (2012) 34–39.
[6] Y. Li, B. Zhang, M. Cheng, Y. Li, L. Hao, H. Guo, Spontaneous arsenic (III) oxidation with bioelectricity generation in single-chamber microbial fuel cells, J. Hazard Mater. 306 (2016) 8–12.
[7] J.A. Cracknell, K.A. Vincent, F.A. Armstrong, Enzymes as working or inspirational electrocatalysts for fuel cells and electrolysis, Chem. Rev. 108 (2008) 2439–2461.
[8] P. Chenevier, L. Mugherli, S. Darbe, L. Darchy, S. DiManno, P.D. Tran, F. Valentino, M. Iannello, A. Volbeda, C. Cavazza, V. Artero, Hydrogenase enzymes: application in biofuel cells and inspiration for the design of noble-metal free catalysts for H_2 oxidation, Compt. Rendus Chem. 16 (2013) 491–505.
[9] Food Energy, Methods of Analysis and Conversion Factors, Food and Nutrition Paper 77, vol. 3, Food and Agriculture Organization of the United Nations, Rome, 2003.
[10] A.T. Yahiro, S.M. Lee, D.O. Kimble, Bioelectrochemistry. I. Enzymeutilizing biofuel cell studies, Biochim. Biophys. Acta 88 (2) (1964) 375–383.
[11] A. Zebda, S. Cosnier, J.P. Alcaraz, M. Holzinger, A. Le Goff, C. Gondran, F. Boucher, F. Giroud, K. Gorgy, H. Lamraoui, P. Cinquin, Single glucose biofuel cells implanted in rats power electronic devices, Sci. Rep. 3 (2013) 1516.
[12] S. Cosnier, A.J. Gross, A. Le Goff, M. Holzinger, Recent advances on enzymatic glucose/oxygen and hydrogen/oxygen biofuel cells: achievements and limitations, J. Power Sources 325 (2016) 252–263.
[13] A.A. Babadi, S. Bagheri, S.B.A. Hamid, Progress on implantable biofuel cell: nano-carbon functionalization for enzyme immobilization enhancement, Biosens. Bioelectron. 79 (2016) 850–860.
[14] A. Zebda, J.P. Alcaraz, P. Vadgama, S. Shleev, S.D. Minteer, F. Boucher, P. Cinquin, D.K. Martin, Challenges for successful implantation of biofuel cells, Bioelectrochemistry 124 (2018) 57–72.
[15] Y. Chung, D.C. Tannia, Y. Kwon, Glucose biofuel cells using bi-enzyme catalysts including glucose oxidase, horseradish peroxidase and terephthalaldehyde crosslinker, Chem. Eng. J. 334 (2018) 1085–1092.
[16] S. El Ichi-Ribault, J.P. Alcaraz, F. Boucher, B. Boutaud, R. Dalmolin, J. Boutonnat, P. Cinquin, A. Zebda, D.K. Martin, Remote wireless control of an enzymatic biofuel cell implanted in a rabbit for 2 months, Electrochim. Acta 269 (2018) 360–366.
[17] X. Xiao, H.Q. Xia, R. Wu, L. Bai, L. Yan, E. Magner, S. Cosnier, E. Lojou, Z. Zhu, A. Liu, Tackling the challenges of enzymatic (bio)fuel cells, Chem. Rev. 119 (16) (2019) 9509–9558.
[18] C. Abreu, Y. Nedellec, O. Ondel, F. Buret, S. Cosnier, A. Le Goff, M. Holzinger, Glucose oxidase bioanodes for glucose conversion and H_2O_2 production for horseradish peroxidase biocathodes in a flow through glucose biofuel cell design, J. Power Sources 392 (2018) 176–180.
[19] X. Huang, L. Zhang, Z. Zhang, S. Guo, H. Shang, Y. Li, J. Liu, Wearable biofuel cells based on the classification of enzyme for high power outputs and lifetimes, Biosens. Bioelectron. 124–125 (2019) 40–52.
[20] Z. Kang, K. Jiao, J. Cheng, R. Peng, S. Jiaoa, Z. Hu, A novel three-dimensional carbonized PANI1600@CNTs network for enhanced enzymatic biofuel cell, Biosens. Bioelectron. 101 (2018) 60–65.
[21] F. Boussema, A.J. Gross, F. Hmida, B. Ayed, H. Majdoub, S. Cosnier, A. Maaref, M. Holzinger, Dawson-type polyoxometalate nanoclusters confined in a carbon nanotube matrix as efficient redox mediators for enzymatic glucose biofuel cell anodes and glucose biosensors, Biosens. Bioelectron. 109 (2018) 20–26.
[22] Ó. Santiago, E. Navarro, M.A. Raso, T.J. Leo, Review of implantable and external abiotically catalysed glucose fuel cells and the differences between their membranes and catalysts, Appl. Energy 179 (2016) 497–522.
[23] Z. Tang, W. Wu, K. Wang, Oxygen reduction reaction catalyzed by noble metal clusters, Catalysts 8 (2) (2018) 65.
[24] M. Łukaszewski, Electrochemical methods of real surface area determination of noble metal electrodes – an overview, Int. J. Electrochem. Sci. 11 (2016) 4442–4469.
[25] V. Oncescu, D. Erickson, High volumetric power density, non-enzymatic glucose fuel cells, Sci. Rep. 3 (2014) 1226.
[26] A. Navaee, M. Narimani, A. Korani, R. Ahmadi, A. Salimi, S. Soltanian, Bimetallic $Fe_{15}Pt_{85}$ nanoparticles as an effective anodic electrocatalyst for non-enzymatic glucose/oxygen biofuel cell, Electrochim. Acta 208 (2016) 325–333.
[27] H.A. Tsang, D.Y.C. Leung, Pd-Pt loaded graphene aerogel on nickel foam composite as binder-free anode for a direct glucose fuel cell unit, Solid State Sci. 71 (2017) 123–129.

[28] J. Chen, H. Zheng, J. Kang, F. Yang, Y. Cao, M. Xiang, An alkaline direct oxidation glucose fuel cell using three-dimensional structural Au/Ni-foam as catalytic electrodes, RSC Adv. 7 (5) (2017) 3035–3042.
[29] A. Janz, A. Köckritz, L. Yao, A. Martin, Fundamental calculations on the surface area determination of supported gold nanoparticles by alkanethiol adsorption, Langmuir 26 (9) (2010) 6783–6789.
[30] M. Xu, Y. Sui, G. Xiao, X. Yang, Y. Wei, B. Zou, Kinetically controlled synthesis of nanoporous and their enhanced electrocatalytic activity for glucose-based biofuel cells, Nanoscale 9 (2017) 2514–2520.
[31] L. Yang, Y. Zhang, M. Chu, W. Deng, Y. Tan, M. Ma, X. Su, Q. Xie, S. Yao, Facile fabrication of network film electrodes with ultrathin Au nanowires for nonenzymatic glucose sensing and glucose/O_2 fuel cell, Biosens. Bioelectron. 52 (2014) 105–110.
[32] X. Liu, Z. Li, Y. Yang, P. Liu, P. Zhang, Electricity generation from a refuelable glucose alkaline fuel cell with a methyl viologen-immobilized activated carbon anode, Electrochim. Acta 222 (2016) 1430–1437.
[33] Y. Zhao, L. Fan, D. Gao, J. Ren, B. Hong, High-power non-enzymatic glucose biofuel cells based on three-dimensional platinum nanoclusters immobilized on multiwalled carbon nanotubes, Electrochim. Acta 145 (2014) 159–169.
[34] G. Zeng, W. Li, S. Ci, J. Jia, Z. Wen, Highly dispersed NiO nanoparticles decorating graphene nanosheets for non-enzymatic glucose sensor and biofuel cell, Sci. Rep. 6 (2016) 36454.
[35] Y. Zhao, X. Liu, X. Wang, P. Zhang, J. Shi, Peony petal-like 3D graphene-nickel oxide nanocomposite decorated nickel foam as high-performance electrocatalyst for direct glucose alkaline fuel cell, Transnatl. J. Hydrogen Energy 42 (50) (2017) 29863–29873.
[36] L. Wang, H. Shao, X. Lu, W. Wang, J.R. Zhang, R.B. Song, J.J. Zhu, A glucose/O_2 fuel cell-based self-powered biosensor for probing a drug delivery model with self-diagnosis and self-evaluation, Chem. Sci. 9 (2018) 8482–8491.
[37] A.M. Mahmoud, T. Tang, D.J. Harrison, W.E. Lee, A.B. Jemere, A regenerating self-assembled gold nanoparticle-containing electrochemical impedance sensor, Biosens. Bioelectron. 56 (2004) 328–333.
[38] M. Pasta, F. La Mantia, Y. Cui, Mechanism of glucose electrochemical oxidation on gold surface, Electrochim. Acta 55 (2010) 5561–5568.
[39] J. Zhou, C. Chakrabarti, K. Lee, N. Chang, S. Vrudhula, Maximizing the lifetime of embedded systems powered by fuel cell-battery hybrids, IEEE Trans. Very Large Scale Integr. Syst. 17 (1) (2009) 22–32.
[40] Y. Zhao, L. Fan, Y. Zhang, Q. Que, B. Hong, Three-dimensional PtxNi1-x nanoclusters supported on multiwalled carbon nanotubes in enzyme-free glucose biofuel cells, J. Power Sources 296 (2015) 30–39.
[41] H. Guo, H. Yin, X. Yan, S. Shi, Q. Yu, Z. Cao, J. Li, Pt-Bi decorated nanoporous gold for high performance direct glucose fuel cell, Sci. Rep. 6 (2016) 39162.
[42] K. Jiao, Y. Jiang, Z. Kang, R. Peng, S. Jiao, Z. Hu, Three-dimensional Co_3O_4@MWNTs Nanocomposite with Enhanced Electrochemical Performance for Nonenzymatic Glucose Biosensors and Biofuel Cells vol. 4, Royal Society Open Science, 2017, p. 170991.
[43] F. Gholami, A. Navaee, A. Salimi, R. Ahmadi, A. Korani, R. Hallaj, Direct enzymatic glucose/O_2 biofuel cell based on polythiophene carboxylic acid alongside gold nanostructures substrates derived through bipolar electrochemistry, Sci. Rep. 8 (2018) 15103.